Composite Structures 308 (2023) 116683

Contents lists available at ScienceDirect

Composite Structures

journal homepage: www.elsevier.com/locate/compstruct

Development and manufacturing of flexible joints based on corrugated composite laminates

Marco Riva [a,*], Alessandro Airoldi [a], Tommaso Turconi [a], Pietro Ballarin [a], Matteo Boiocchi [a], Luigi Bottasso [b]

[a] Department of Aerospace Science and Technology (DAER), Politecnico di Milano, Via La Masa, 34, 20156 Milan, Italy
[b] Leonardo Helicopters Division, Via Giovanni Agusta, 520, 21017 Samarate, VA, Italy

ARTICLE INFO

Keywords:
Composites
Corrugated laminated
Flexible joints
Manufacturing
Morphing
Rotorcraft transmission

ABSTRACT

This paper investigates the exploitation of corrugated composite laminates to design flexible joints. The joint can sustain axial load using a flexible frame integrated into a composite tube, which transmits torque and supports the frame allowing significant bending deformations with low bending stiffness. The concept is explored numerically and applied to the design of a heavy-duty flexible joint for rotorcraft. The element is required to transmit torque, allow misalignments, and withstand high compressive forces in emergency landing conditions. After preliminary design, a manufacturing technique is developed to produce axisymmetric corrugated laminates. Technological demonstrators are produced and subjected to tests, investigating the failure modes, validating the numerical approach for predictions, and confirming the quality of manufacturing. Finally, a complete prototype is designed in detail, produced, and then tested in bending and compression. The results, in agreement with the numerical analyses, confirm the capability to withstand design limit loads without damage development.

1. Introduction

The design solutions for a structural joint, which transmit forces between rotating parts or parts undergoing relative displacements, typically involves the adoption of quite complex mechanisms, which couple selectively the degrees of freedom of the parts connected. A different strategy can be devised by exploiting the properties of materials and structures with stiffness variable in different directions, so to develop a kind of hingeless joint that combines the possibility of relative motions in given directions, with a non-zero but relatively low stiffness, with the capability to transmit the required loads in other directions. The design of such flexible joints can nowadays take advantage of the studies that have been performed in recent years, aimed to develop flexible structures with the capability to deform seamlessly and progressively in controlled modes and directions. In particular, innovative solutions have been studied for morphing aerospace elements, with the aim of replacing classical control surfaces based on mechanisms, thus improving aerodynamic efficiency, and allowing a continuous optimization for the different phases of the missions [1–7]. The design process of these morphing components can be particularly demanding, since it is required to obtain a component characterized by high flexibility associated to the deformation in prescribed modes, while at the same time retaining high stiffness and strength to transmit the aerodynamic loads to the primary structures. These conflicting requirements, which are analogous to those characterizing a flexible joint, can be fulfilled by exploiting the properties of materials and of innovative structural architectures to obtain high anisotropic responses.

Among the structural geometries considered for morphing application, promising candidates to design parts that combine flexibility in given directions with load carrying capability in other directions are represented by corrugated laminates [8–14], which are characterized by a highly orthotropic response in terms of both stiffness and strength. Corrugated sheets exhibit tunable properties in the direction of the corrugated profile, which can be considered their morphing direction, by using different corrugation profiles, and excellent stiffness and strength in the other non-morphing directions [15]. The application of composite materials to a corrugate geometry allows a further increment of the intrinsic tunability and anisotropy of the corrugate by properly selecting the lay-up characteristics ([16,17]). Composite materials are also particularly suitable for morphing application due to their ability to

* Corresponding author.
E-mail address: marco2.riva@polimi.it (M. Riva).

https://doi.org/10.1016/j.compstruct.2023.116683
Received 13 October 2022; Received in revised form 12 December 2022; Accepted 7 January 2023
Available online 9 January 2023

undergo large deformation without failure and their high fatigue resistance properties in the fiber direction, which allows them to change their shape several times without nucleating damages or cracks. Moreover, they are particularly indicated for aerospace usage since they allow the design of lightweight components, which is a highly valuable characteristic in this application field.

The properties of composite corrugated laminates have been exploited to develop structural component with the capability of a progressive shape variation in predefined directions. Significant examples can be the usage for actuated morphing skins, such as in [8,9,16]. The possibility to host diffused actuator systems has been also explored, by integrating shape memory alloys wires (Nitinol), which act directly on the flexible component [17–19].

Following these evaluations, composite corrugated laminates in axisymmetric configuration have been considered for the development of joints that are flexible in the bending direction, but retain the capability to transmit torque, lateral loads and to sustain also axial loads. Actually, some solutions for flexible joints based on corrugated geometry can be found [20–22], while similar solutions can be obtained by adopting helical geometries [23]. These types of joints can accommodate large misalignments between rotating shafts also adopting several joints connecting multiple shaft segments [24]. Different concepts for flexible joints are presented in [25], where the joint works as a rope in which the interlacement allows the flexibility required, and in [26] in which a flexible shaft rotates inside a hose, and it is stabilized by several bearings. However, most of the proposed flexible joints carry relatively low loads and all of them combine bending flexibility with the capability of transmitting torque. The transmission of other types of loads, such as axial or transverse loads is not required.

Composite technology and the properties of corrugated composite laminates have been exploited in this work to develop a heavy-duty flexible joint for rotorcraft power transmission, with particular severe requirements and innovative characteristics with respect to the solutions for flexible joints presented in literature.

The type of joint studied in this work shall meet more challenging requirements, which arise for particular applications in rotorcraft transmissions, where joints have to transmit very high loads including torque, axial compressive, tensile and transverse force, which have to be transmitted between parts subjected to relative motion or displacement. Actually, the inherent lightweight and flexibility of modern rotorcraft structures and the complexity of rotorcraft transmissions requires the accommodation of misalignment angles and change of direction in power shafts, which could represent several appealing application scenarios for innovative heavy-duty flexible joints, since the state-of-the-art solutions are represented by metallic gimbal joints, which involves complex, lubricated mechanism with considerable weight, requiring high maintenance effort.

Accordingly, the development of a solution for a flexible structural joint represents a relevant goal and it can be pursued by applying the concept of load path separation, which is one of the key strategies for the development of morphing structures with load carrying capabilities. In particular, in the solution proposed, the axial load is transferred by a metallic frame, while the torsional load is reacted by a composite tubular structure which is corrugated in order to allow bending deformation with a reduced and tunable stiffness. Bending flexibility is obtained by adopting a corrugated shape for the composite structure combined with a metallic frame with a geometry providing high axial stiffness and strength but very low overall bending stiffness.

The manufacturing of such a type of joint requires the production of axisymmetric corrugated laminates, which is particularly challenging if high curvatures due to the corrugated profile and to the axisymmetric shape are involved. The double curvature of axisymmetric corrugated geometry is expected to amplify the difficulties of producing corrugated laminates, which are reported in literature [9,10,15,16] and can be addressed by following step-by-step lamination procedures and using properly designed counter-molds to control pressure exertion during curing. Therefore, both design and manufacturing issues have to be addressed to obtain a realistic and successful solution for practical applications.

Moreover, the adoption of a composite corrugated laminate for a primary structure of a rotary wing vehicle requires a painstaking evaluation of the state of stress and very reliable predictions regarding the failure modes of the corrugated laminate, which can be influenced not only by the in-plane stress components in the plies [27], but also by out-of-plane stress states, particularly in the zones presenting high curvatures [28].

The work is articulated in four chapters: the first one describes the initial numerical studies performed to verify the structural response that can be achieved by the design concept in terms of maximum bending angle and maximum compressive sustainable load. Then, in the second part, a realistic heavy-duty application scenario is considered, and the preliminary design of the component is carried out to comply with the prescribed requirements, taking into account the technological limitations related to the production of the axisymmetric laminates with double curvature. In the third part, an insight into the technological process is presented. A full description of the manufacturing procedures is provided, and the quality of the laminate is assessed by testing a specimen obtained from the produced element. Experimental outcomes are also compared with the results of finite element analyses, to validate the design approach and investigate the real failure modes. Finally, the last chapter concerns the detailed design and assembly to produce a prototype of the joint, which was subsequently tested in bending and in compression.

2. Structural concept and preliminary FEM studies

2.1. Flexible corrugated joints with load carrying capability

The concept presented in this work is based on the application of composite corrugated laminates to the design of a flexible joint capable of sustaining considerable axial load, significant torque, while maintaining low weight and the capability to undergo a bending deformation with a relatively low bending stiffness. It is known that a corrugated tube is inherently capable of carrying significant torsional loads, but it cannot sustain axial loads without undergoing significant elongation in tension or collapse in compression.

The design of the joint proposed in this work is based is the possibility to carry axial loads through a separate load path characterized by relatively thin lateral stiffeners, with adequate axial stiffness and strength and low stiffness when bent out of their plane. These thin stiffeners are inherently prone to instability when compressed, but the interaction with the composite corrugated tube provides a lateral support, thus greatly increasing their buckling load. Hence, the integration of the stiffeners in the corrugated tube leads to a module with a high bending compliance when bending moment is applied about an axis that lies on the plane of the thin lateral stiffeners. However, if two modules are connected with mutually orthogonal stiffener planes, a joint with a high compliance in all bending directions is obtained. The resulting scheme is exemplified in Fig. 1b and c where each module can bend with a relatively low stiffness along one axis, X_1 and X_2, respectively, so that the combination of the two modules makes possible bending in a generic direction.

Accordingly, high bending compliance is combined with the possibility of carrying both axial and torsional loading. The stiffeners are fundamental to carry the axial load, but the corrugated tube provides a lateral support for the stiffeners, increasing the axial buckling load of the whole assembly. The transfer of the axial load to the system of mutually orthogonal stiffeners is achieved through a system of annular diaphragm, at the ends of each module. Finally, the closed section corrugate tube is essential to sustain the torsional load.

In real life operations, system of forces can be simultaneously applied to the joint leading to complex loading conditions, but the load path

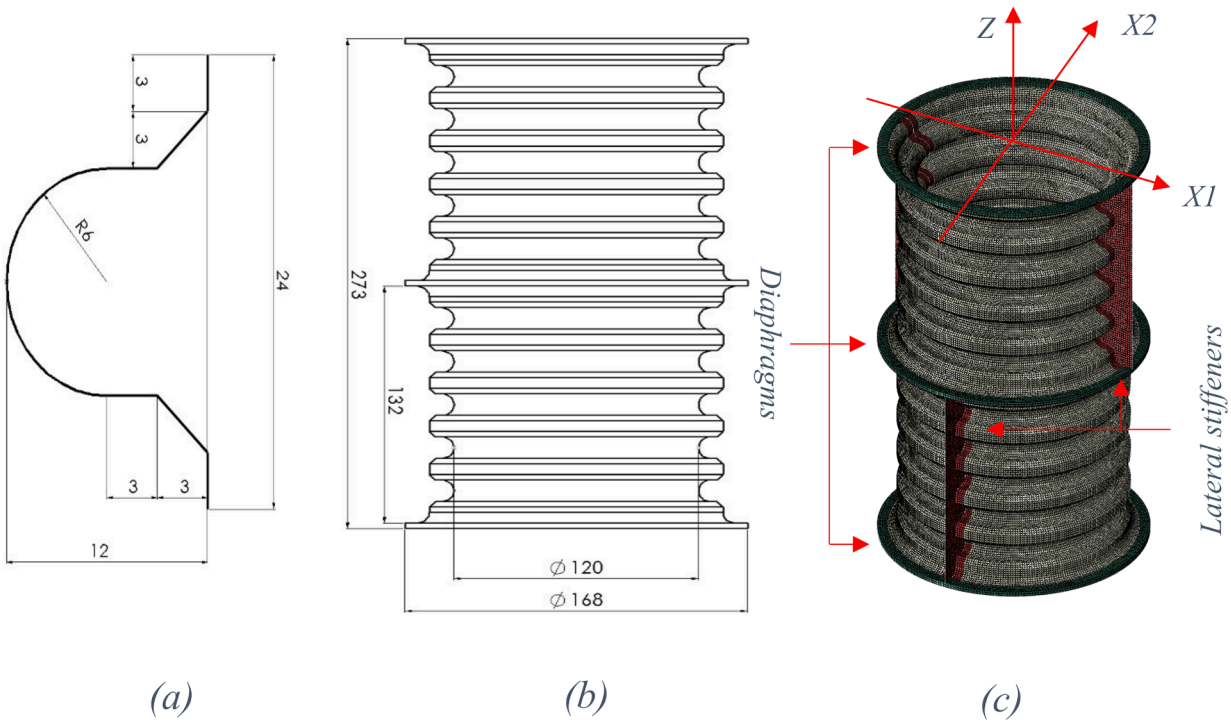

Fig. 1. (a) Shape and dimension of the corrugation scheme; (b) Dimension and shape of the whole tube; (c) FE model of complete joint based on corrugated laminate.

separation should ensure the component capability to sustain the loads. Moreover, it is expected that the joint is capable of transmitting significant transverse loads, along X_1 or X_2 axis, without excessive shear deformations.

2.2. Preliminary FEM analyses of the concept

Some numerical analyses were performed to assess the potential of the concept in terms of axial compression strength and maximum achievable bending. The configurations studied were based on the one showed in Fig. 1, representing a corrugated tube divided in two modules stiffened along two mutually orthogonal planes, which were delimited by three diaphragms.

Two different geometries were considered, with module height equal to 132 mm and 84 mm, respectively. Both geometries had identical square-rounded corrugation profiles, shown in Fig. 1a with a period of 24 mm and a depth of 12 mm. The profile was chosen considering the experience gained in previous works on plane corrugated panels [16,17], where it exhibited remarkable properties in terms of maximum elongation and flexibility.

Finite element models were developed and solved by using Simulia/Abaqus solver code. Reduced-integration shell elements (*S4R and S3R elements* [29]) with typical size of 1.5 mm were used for the corrugate and the stiffeners, while continuum shells (*SC8R elements* [29]) were used for the diaphragms. The mesh of the corrugated tubes and that of the stiffeners were connected by using a TIE algorithm, available in the solver code to join dissimilar meshes. The complete model consisted of 99,448 shell elements and 7296 continuum shell elements for a total number of 625,206 nodal degrees of freedom in the longer configuration and for the shorter configuration the model consisted of 65,160 shells and 7296 continuum shells, totaling 418,734 variables.

Two loading conditions were defined to evaluate both the critical load under axial compression and the stress state for a bending corresponding to a deflection angle of 7° between the end diaphragm, which were modelled as rigid bodies. The bending analyses allowed the evaluation of the bending stiffness and of the stress state for the imposed deflection, so the assess the structural integrity of the composite joint under bending.

Different layups were considered for the composite parts. In particular, a variable $[45_n / 0_m / 0_m / 45_n]$ layup was considered for the corrugated tube, by using Carbon-reinforced fabric or Glass-reinforced fabric with polymeric matrix composite materials, with the characteristics are reported in Table 1. The stiffeners were designed to be constituted by a polymeric core reinforced by a variable number of carbon fabric plies on both sides, so to vary the bending stiffness of the element. In particular 1, 2, and 3 plies of carbon fabric were considered, so to obtain a reinforcement thickness of 0.22 mm, 0.44 mm, and 0.66 mm on each side of the polymeric core. The properties of the polymeric core were based on the ones of a polyimide material, with a Young modulus equal to 1650 MPa, Poisson ratio of 0.3 and a thickness of 1.0 mm [30]. The central diaphragm between the two modules was modelled by considering a ring with a thickness of 3 mm, an external diameter of 168 mm, and an internal diameter of 156 mm, made of metallic material with a Young modulus of 73,000 MPa and a Poisson's ratio of 0.33. The diaphragm at the ends of the joint were modelled as rigid bodies. The lower one was clamped. The upper one was left free to rotate in the buckling analysis, with the axial load applied in the vertical direction and the translation along X_1 and X_2 directions kept fixed. In the bending analysis a rotation of 7° was imposed about axis X_1, without applying constraints to the other degrees of freedom.

The results of the preliminary evaluations, reported in Table 2, confirmed the potential of the concept. The critical load under axial compression, P_{cr}, was influenced by the lay-up of the lateral stiffener, as it can be seen by comparing the results obtained with the same lay-up of the tube. However, a significant and even greater increment was obtained by varying the lay-up of the tube, thus indicating the role of the corrugated tube in supporting the thin stiffeners. Actually, two typical buckling modes were found in correspondence of the critical load, which are represented in Fig. 2. Type *A* buckling (Fig. 2a) was obtained with the more compliant lay-ups. It occurs at a relatively low P_{cr}, with a buckling mode involving all the central part of the assembly (corrugated tube, diaphragm, stiffeners). If the tube wall exceeded a certain stiffness threshold, type *B* buckling occurs (Fig. 2b), which is a local mode in the stiffeners, characterized by a higher P_{cr}. The height of the module had a

Table 1
Material characteristics of preliminary numerical tests.

	E_{11} (MPa)	E_{22} (MPa)	ν_{12}	G_{12} (MPa)	G_{13} (MPa)	G_{23} (MPa)	Thickness (mm)
Carbon	63,000	63,000	0.055	5500	2500	2500	0.22
Glass	23,000	23,000	0.055	5500	2500	2500	0.25

Table 2
Results of the numerical analysis for the two geometries, with varying material, lay-up, and thickness of reinforcement layer applied to lateral stiffeners.

	Case	Tube Material	Tube lay-up	Thickness of reinforcement applied to the stiffeners [mm]	P_{cr} [N]	Buckling mode	K_b [Nm/°]
1st geometry	1.1	Carbon	[45/45]	0.22	5303	A	3.06
	1.2	Carbon	[45/45]	0.44	5709	A	3.13
	1.3	Carbon	$[45/0]_s$	0.22	8173	B	18.63
	1.4	Carbon	$[45/0]_s$	0.44	15,249	B	18.96
	1.5	Carbon	$[45/0]_s$	0.66	22,971	B	19.17
	1.6	Glass	$[45/0]_s$	0.22	7367	B	11.36
	1.7	Glass	$[45/0]_s$	0.44	13,765	B	11.53
2nd geometry	2.1	Carbon	[45/45]	0.22	5460	A	37.3
	2.2	Carbon	[45/45]	0.44	5877	A	38.3
	2.3	Glass	$[45/0]_s$	0.22	8109	B	137.9
	2.4	Glass	$[45/0]_s$	0.44	14,946	B	140.3
	2.5	Glass	$[45/0]_s$	0.66	19,413	A	142.2

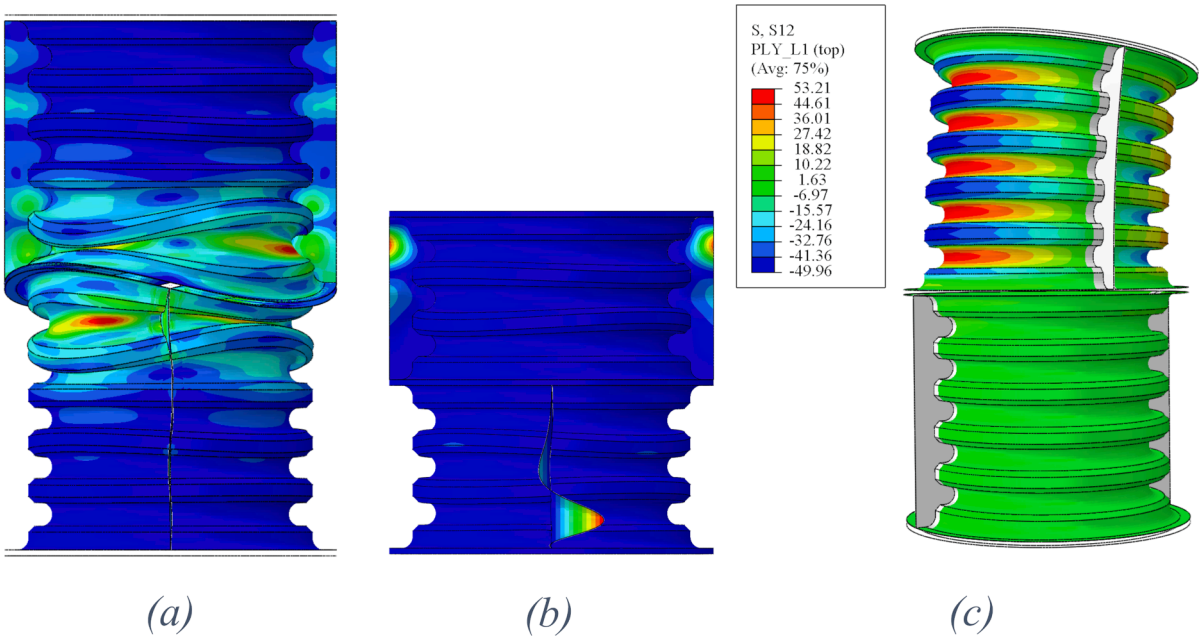

Fig. 2. (a) Buckling mode A on the first geometry (configuration 1.1), (b) Buckling mode B on the second geometry (configuration 2.4), (c) Shear stress in 45° ply in bending for configuration 1.5.

relatively small influence on P_{cr}, since the difference between the results referred to the long and short module configuration was less than 10%, all the other parameters being equal.

The bending stiffness of the element was strongly influenced by the tube lay-up and was almost independent from the stiffeners lay-up. Moreover, the adoption of glass reinforced material in the tube could lead to reduce bending stiffness, while still providing an adequate support to the stiffeners, as indicated by the level of compressive buckling load. The short module configuration has a significantly higher bending stiffness than the long module one, indicating a fundamental role of the joint height on the bending compliance.

The state of stress in the plies in the bending analysis with imposed 7° deflection is not reported in detail for the sake of brevity. A contour for the long module of τ_{12} stress is exemplified in Fig. 2c. The maximum state of stress for the configurations using carbon was obtained for case #1.5 with $\sigma_{11} = 272.4$ MPa, $\tau_{12} = 53.8$ MPa, while for glass configurations it was found for case 1.7 with $\sigma_{11} = 126.2$ MPa, $\tau_{12} = 58.9$ MPa. Considering the typical strength properties of composite plies at the lamina level, the in-plane shear stress τ_{12} is the most significant component for the risk of failure. However, the values are lower of the typical strength values found in composite materials for aerospace applications [31]. Hence, achieving a 7° deflection is well within the capabilities of this joint configuration. The stress state a 7° of bending deflection is more severe for short module configuration, as it could be expected, with maximum values of stresses in carbon configurations of $\sigma_{11} = 221.9$ MPa, $\tau_{12} = 80.6$ MPa and of $\sigma_{11} = 219.5$ MPa, $\tau_{12} = 103.3$ MPa for glass configurations, obtained for case 2.2 and 2.5 respectively. In such a case, the stress state is likely to exceed the linearity limit of the laminates.

Overall, the results indicate that the hypotheses at the base of the

concept are verified, with the buckling load of the component that was greatly influenced by the presence of the corrugate. The axial load level that can be supported is significant. Taking as an example configuration #1.5 presented in Table 2, a critical load exceeding 22 kN was obtained, while keeping the bending stiffness below 20 Nm/°. In general, the concept showed the need of a trade-off between the critical load and the bending stiffness and a trade-off between the length of the module and the maximum achievable bending deflection in the elastic range.

Moreover, these numerical results also proved a remarkable design flexibility of the concept. Indeed, bending stiffness, maximum deflections and axial load carrying capability can be varied by acting on the overall size, lay-up of the corrugated tube, and stiffener thickness and material. The choice of the corrugation profile is also expected to have a great influence on the mechanical response, even if it was not considered in the parametric studies presented.

However, these preliminary evaluations do not take into consideration the technological feasibility of the joint, which can result significantly complex, particularly when small size, deeply corrugated profiles and complex lay-ups of the tube walls have to be produced. Such aspects will be considered in the next section, where the concept is applied to design and manufacture a joint for a defined application scenario.

3. Application of the concept to a specific design case

3.1. Design case and adaptation of the concept

The appreciable results obtained in the preliminary studies motivated the development of a joint for a specific design case, which is

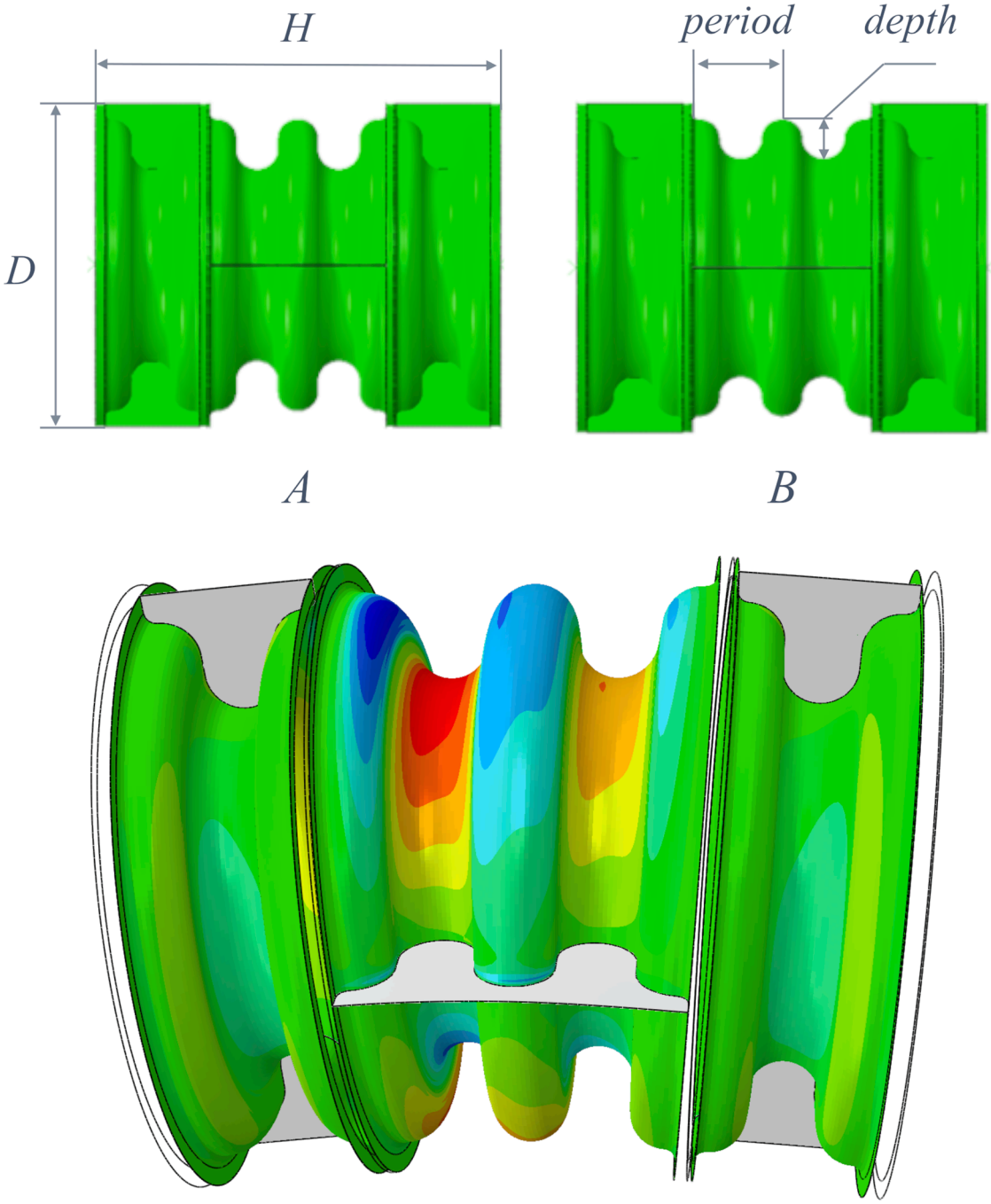

Fig. 3. Proposed geometries (A and B) for the heavy-duty joint and a deformed configuration under limit loading.

represented by a heavy-duty flexible joint for an aeronautical application. The component was intended to substitute a metallic universal joint inside a rotorcraft transmission system. The joint connects two parts transmitting significant load levels, while the parts are mounted on flexible structures, so that small misalignments have to be taken into account. The specific component is a non-rotating joint that provide the reaction to the torque transmitted by a coaxial rotating shaft. In limit conditions, the element is subjected to significant axial, torque and lateral load components. Moreover, it also performs critical roles in emergency landing conditions, thus leading to severe requirements in terms of axial load carrying capability. Hence, two main conditions were considered: a limit operational condition and an extreme condition, which is representative of an emergency landing and must be sustained once in a lifetime. The element was required to sustain the limit condition allowing a 1.4° misalignment. The bending stiffness of the joint should be minimized, and, in any case, the misalignment angle has to be reached with a moment lower than the applied torsional load. Overall, the specific design case is characterized by significant load values and relatively low displacement, thus indicating the need for high thickness in the composite tube and in the lateral stiffener, which are conflicting with the objective of reducing the bending stiffness. To complete the requirements a limit on the maximum dimensions was introduced, with a height of H and a diameter of D. Moreover, due to the proposed aeronautical application, keeping a low weight was fundamental.

3.2. Definition of the design configuration

To meet the expected requirements, the numerical approach developed for the preliminary studies presented in section 2 was applied to identify a design configuration, which was detailed in the subsequent phases of development. The preliminary studies led to a basic lay-out, showed in the two configurations reported in Fig. 3, which were characterized by three modules: two short ones at the extremities and one long one in the middle. The stiffener plane was the same for the short modules, while for the central module the stiffeners plane was shifted by 90° with respect to the one of the short modules. The technological feasibility was taken into account since the early design phases, leading to avoid excessively small curvature radii of the surfaces to simplify the lamination process. Hence, the corrugation period was increased, and a rounded profile was adopted, which was considered technologically more feasible and less prone to delamination phenomena with respect to the square-rounded profile considered in section 2, due to higher radii of curvature. Following the indication of the preliminary studies, glass-fiber reinforced materials was selected for the development of the joint. Finally, the stiffeners and the diaphragms were designed to be produced by using a metallic alloy, to simplify the manufacturing process and to increase the strength to sustain high axial loads.

A sensitivity study performed on different combinations of period/depth ratio and lay-up of the composite corrugated tubes and consideration based on technological feasibility led to identify-eight promising configurations that were analyzed in detail. These were a combination of two possible geometries, denoted as A and B in the following, and four possible lay-ups.

The two proposed geometries, A and B, are shown in Fig. 3. Geometry A had a period to depth ratio of 1.54, while B had a period/depth ratio equal to 2.00. The four selected lay-ups, numbered 1 to 4, were composed by Glass/Epoxy Fabric and Unidirectional composite material, with the material characteristics are reported in Table 3. Preliminary laminations tests indicated that the fabric ply could be more easily draped on the double-curvature surface when oriented at ±45° with respect to the tube axis. Hence, fabric plies could have been used for the external layers of the lay-up, while internal reinforcement could be obtained by using unidirectional plies. Accordingly, the lamination sequence was of the type [FB45°/UD0°/UD90°/UD0°/FB45°]. The difference between the 4 lay-ups considered in the sensitivity study was based on the thickness of the different block of plies with different orientation. In particular, the configurations considered are presented in the following list:

1. reference thickness configuration type [FB45°/UD0°/UD90°/UD0°/FB45°].
2. thickness of FB45° plies increased by 50%.
3. thickness of UD0° plies increased by 50%.
4. thickness of UD90° plies increased by 50%.

The finite element models of the 8 configurations were developed by using about 110,000 shell elements (*S4 elements* [29]) and about 22,000 continuum shell elements (*SC8R* elements [29]) with typical size in the range 1.2 mm ÷ 1.8 mm, for a total number of about 766,000 nodal degrees of freedom.

The bending stiffness and the critical load were evaluated by using the same type of boundary conditions applied in the preliminary studies. The results are reported in the two histograms in Fig. 4 and are normalized with respect to two limits derived from the requirements. Fig. 4a is referred to critical load, where a limit is set to a value that guarantees a significant margin of safety to carry the axial load in extreme conditions. Fig. 4b reports the bending stiffness, with a limit set to the value that correspond to a bending moment for 1.4° deflection equal to the applied torsional load in limit conditions. The analysis of results indicates that geometry A provided the best solutions, since it satisfied the minimum critical load requirement, with a significantly lower bending stiffness than configuration B. However, it should be noted that geometry A has the deepest corrugation, so that lamination is expected to be more critical than in the case of geometry B.

Regarding the effect of the lay-up on the performances, it can be seen that the higher is the critical load, the higher is the bending stiffness. However, all the proposed lay-ups satisfy the imposed limits on these performances and the selection require a more detailed evaluation of the state of stress in limit and extreme conditions.

Accordingly, two sets of loads were introduced, corresponding to the limit and ultimate conditions, with values reported in Table 4. The limit load set was a combination of axial, torsion, and bending load, while the ultimate load conditions was a composed by a very high axial load combined with a torsional load and was representative of an emergency landing condition.

All the eight possible configurations were numerically tested under the two conditions, using a maximum stress criterion to verify the strength of the element. The criterion was set up assuming the design values reported in Table 5, for both the fabric and the unidirectional. Such design values were obtained by introducing knockdown factors on the strength allowables defined for the materials.

The results indicate that the fulfilment of strength requirement in limit conditions is not straightforward. The maximum stress states were found in the crest and the valleys on the tensed side of the corrugated profile, as shown in Fig. 3. The most promising configurations were obtained by increasing the thickness of 0° oriented plies (3rd configuration) for both the geometries A and B. The maximum values of stress components are provided in Table 6, normalized with respect to the

Table 3
Material characteristics.

	E_{11} (MPa)	E_{22} (MPa)	ν_{12}	ν_{13}	ν_{23}	G_{12} (MPa)	G_{13} (MPa)	G_{23} (MPa)
Fabric	23,000	23,000	0.11	0.3	0.3	5000	2500	2500
Unidirectional	45,000	13,000	0.25	0.25	0.3	5000	5000	5000

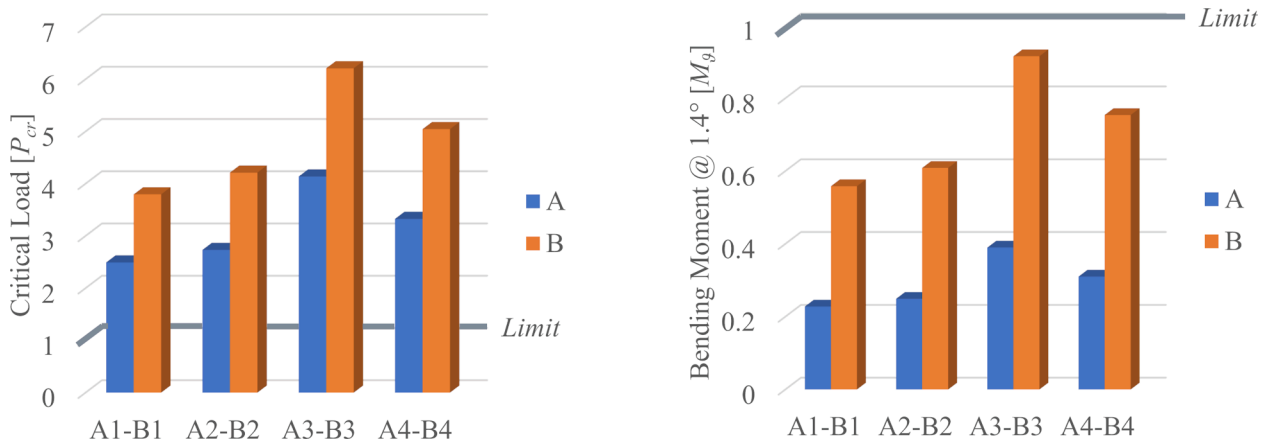

Fig. 4. Sensitivity study of critical load and bending for the different configurations.

Table 4
Loading conditions.

Condition	Nodal degree of freedom					
	U_z	U_{x1}	U_{x_2}	UR_z	UR_{x1}	UR_{x2}
Limit	*-F*	*0.735F*	–	M_ϑ	*1.4°*	–
Ultimate	*−5.275F*	–	–	$1.281M_\vartheta$	–	–

Table 5
Allowables values.

	X_T (MPa)	X_C (MPa)	Y_T (MPa)	Y_C (MPa)	S_{12} (MPa)
Fabric	500	350	500	350	33
Unidirectional	750	500	30	100	33

Table 6
Ply maximum stress levels for A3/B3 configurations in limit load conditions normalized with respect to the corresponding allowable.

		Positive			Negative		
		σ_{11}	σ_{22}	σ_{12}	σ_{11}	σ_{22}	σ_{12}
A3	45°	0.088	0.154	0.909	−0.169	−0.074	−0.818
	0°	0.137	0.900	0.273	−0.162	−0.300	−0.697
	90°	0.153	**2.467**	0.606	−0.238	−0.080	−0.182
	0°	0.137	**1.300**	0.152	−0.162	−0.390	−0.545
	45°	0.188	0.114	0.545	−0.131	−0.234	−0.697
B3	45°	0.064	0.104	0.879	−0.134	−0.066	−0.667
	0°	0.121	0.933	0.242	−0.132	−0.230	−0.545
	90°	0.157	0.267	0.515	−0.186	−0.060	−0.212
	0°	0.115	**1.333**	0.182	−0.120	−0.310	−0.485
	45°	0.168	0.120	0.333	−0.111	−0.020	−0.545

design values reported in Table 5. The stresses in fiber direction are well below the assumed limits, while a couple of plies exhibit stress higher than the design values for matrix-dominated directions.

Given the obtained results, a geometry A, with a lay-up configuration type 3, was selected for further developments. In particular, the technological feasibility of the double-curved corrugated laminate, the experimental investigation of failure modes, and a more detailed stress analysis were carried out before the manufacturing of a joint prototype.

4. Manufacturing and testing of composite axisymmetric corrugates

4.1. Manufacturing process

The main advantage of the selected geometry A was the possibility to minimize the bending stiffness. Nevertheless, it was also characterized by the lowest period/depth ratio, thus complicating the lamination process on the doubly curved geometry. To ensure the feasibility of the manufacturing process, a series of technological tests were carried out. It was decided to produce only half-tube corrugated modules, avoiding the complications involved in the production of hollow tubes, which would have required complex molds made of different parts for extraction or the adoption of soluble mandrels. Hence, it was decided to exploit the presence of the metallic frame to join the half tubes and to carry out the final assembly of the joint.

Focusing on the composite corrugate production, the starting point was to enhance the methodology presented in [16] for the lamination of corrugated panels, which was defined for an element with a single curvature. The technological trials performed in [16] showed that using two metallic molds could led to low quality components, so the proposed method used a metallic mold and an elastomeric counter mold. However, the preliminary design led to define a quite complex lamination sequence production of a double-curved corrugated element with a lamination sequence $[45_n/0_k/90_h/0_k/45_n]$, with $2n$ layers of fabric glass-reinforced plies, oriented at 45°, and $2k + h$ layers of unidirectional glass reinforced plies, oriented at 0° and 90°. The lamination of such laminate on the doubly curved surface resulted far more complex than that of a more conventional corrugated laminate. In particular, the following critical issues had to be addressed:

- direct lamination on a curved mold was found unfeasible, so that the process was based on the preliminary lamination of flat corrugated sub-laminates, followed by a pre-forming according to a doubly curved geometry and by the final depositions of the sub-laminates on a metallic corrugated axisymmetric mold.
- the relatively thick and multi-directional lay-up was found particularly difficult to be stretched and pre-formed, so that the lamination process was divided into three steps: the pre-forming and the deposition of a $[45_n/0_k]$ sub-laminate, the application of 90° layers, the pre-forming and the deposition of the final $[0_k/45_n]$ sub-laminate.
- the deposition of the 90° oriented layers on the whole surface of the tube was unfeasible, so that such layers were applied only in the crest and in the valley of the corrugated laminate, where the stress state was expected to be more critical (see Fig. 3); accordingly, in the final technological trial the tube was laminated according to a lamination $[45_n/0_{2k}/45_n]$ in the flat segments of the corrugated profile and a lamination $[45_n/0_k/90_h/0_k/45_n]$ in the crests and the valleys of the corrugation.

The accomplishment of the process required the production of a series of tools, which are presented in Fig. 5: a set of single-curvature elastomeric molds and counter-molds for pre-forming (Fig. 5c),

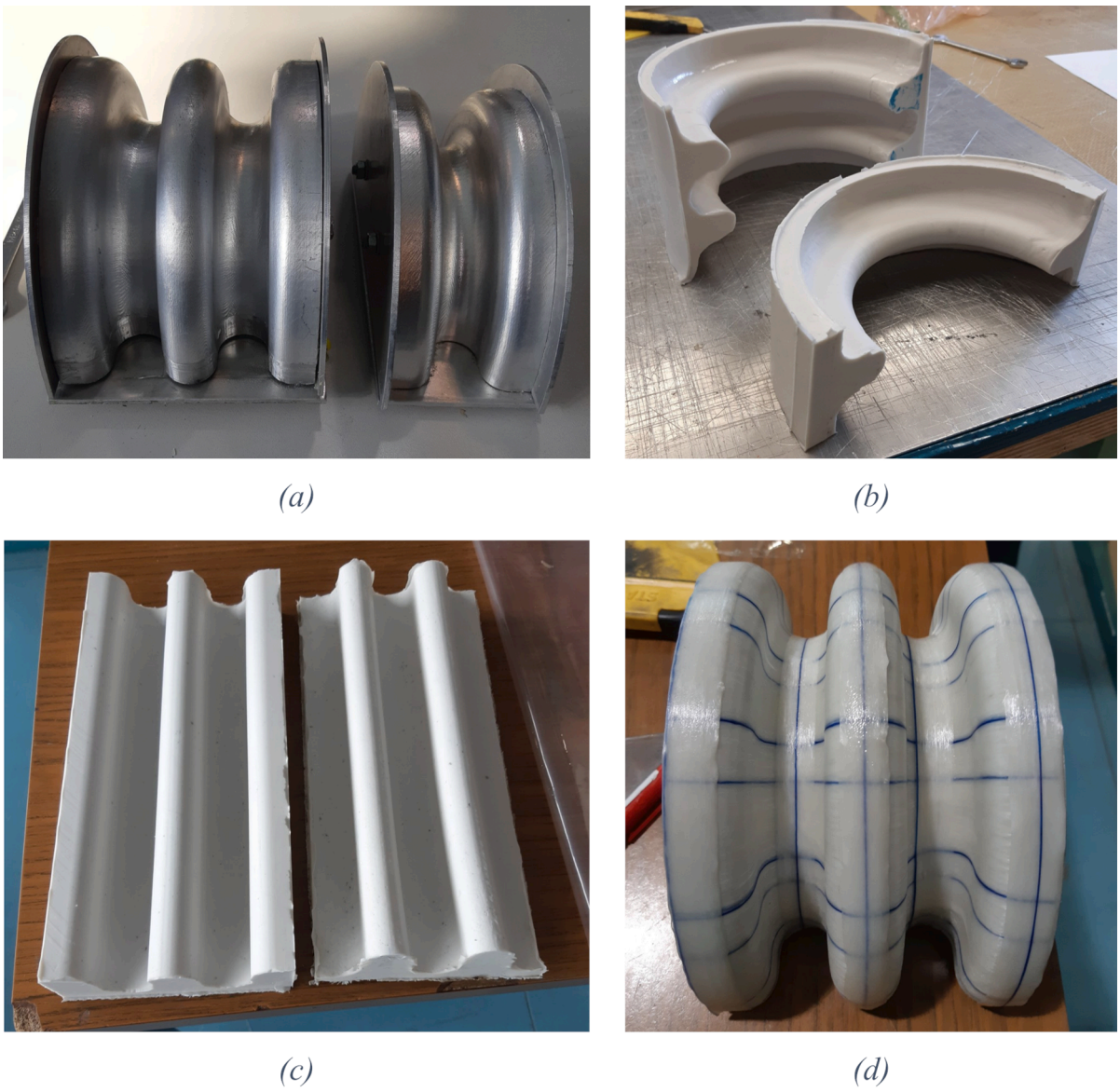

Fig. 5. (a) Metallic molds; (b) and (c) Elastomeric tools; (d) Half laminate with stripes at 90° applied.

metallic molds for the for the curing of the half-tubes related to the central and to the end modules (Fig. 5a), and the corresponding elastomeric counter molds for the accomplishment of vacuum bag technology (Fig. 5b). All the elastomeric tools were produced by using a Two-Part Room-Temperature-Vulcanizing Silicone Rubber (RTV-2).

The set-up of the process eventually led to the following lamination procedure:

i. the pre-preg plies were cut and laminated in a plane rectangular configuration, thus obtaining a $[45_n/0_k]$ sub-laminate.
ii. the initial corrugation was given to the sub-laminates by pressing them between the single-curvature elastomeric molds and counter-mold (Fig. 5c).
iii. the sub-laminates were pre-formed with a curvature in the circumferential direction without extracting them elastomeric tools, by bending the package over a cylindrical surface.
iv. the preformed sub-laminates were extracted from the elastomeric tools and laid on the metallic mold (Fig. 5a), which was previously treated with a releasing agent, removing manually the wrinkles and cutting the lateral borders exceeding the surface of the metallic mold.
v. the $[45_n/0_k]$ lay-up was compacted by applying the elastomeric curved counter-molds and introducing the assembly in a vacuum bag.
vi. after the compaction the $[90_h]$ strips were cut and applied on the laminate; then another compaction cycle was performed on the package; the picture in Fig. 5d shows the results obtained at the end of this phase.
vii. the first two steps were then repeated for the $[0_k/45_n]$ lay-up; the preformed sub-laminate was stretched and laid directly on the $[45_n/0_k/90_h]$ sub-laminate, already positioned on the mold.
viii. the complete laminate was compacted in a vacuum bag and then cured in autoclave for 90 min at 120 °C, with a pressure of 3 bar.

The component obtained showed good surface quality, without excessive wrinkles or resin accumulation. The final component is shown in Fig. 6, where the different lay-up regions are highlighted.

4.2. Tensile testing of a corrugated strip and assessment of the modelling approach

Once the final manufacturing procedure was defined and assessed,

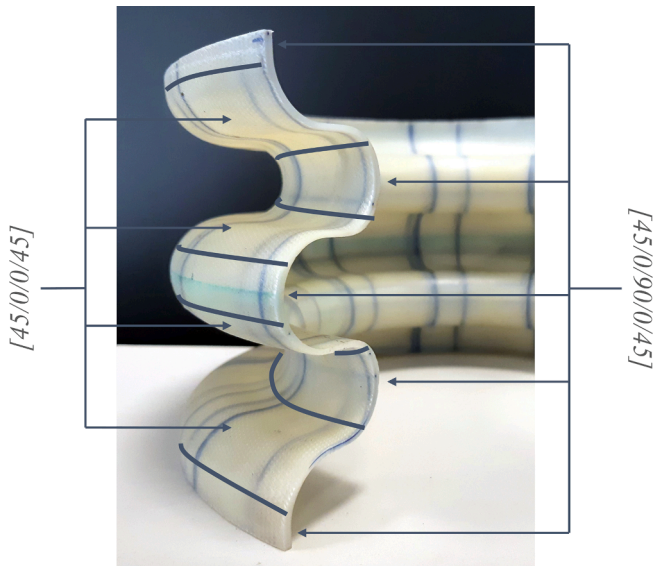

Fig. 6. Final configuration corrugated element with relative lay-up.

two axial traction tests were performed on two strips cut from the corrugate laminate manufactured. The tests aimed at partially reproducing the working condition of the corrugate when the joint was subjected to bending and had multiple objectives, namely the verification of the quality of the manufacturing process, the investigation of the failure modes, and the assessment of FE model predictions related to stiffness and strength.

Two strips were cut from the half-tube produced with a width corresponding to a 16° circular sector of the corrugated tube. The application of the loads to the double-curved ends required the development of special clamps, made of a U-shaped and a *T*-shaped aluminum alloy parts, which were bonded together. Each end of the corrugated strips was sandblasted, inserted, and kept in position into the U-shaped profile. The open sides of the U-shaped profile were closed with and adhesive tape and positioned vertically. Then, epoxy resin was poured to clamp the strips, providing to keep them vertical with respect to surface of the resin. Once the resin curing process was complete, the procedure was repeated with the other end. The result obtained is shown in Fig. 7, which presents one of specimen during the test. The stem of *T*-shaped was inserted into the grips of an MTS 810 testing system to perform a quasi-static tensile test, where an imposed velocity of 1 mm/min was applied up until the failure of the specimen.

The force versus displacement curves obtained in the two tests are reported in Fig. 10. Both specimens widely exceeded the expected displacement for the corrugated laminates in the design condition of the joint, evaluated considering the maximum bending angle. Such limit is represented by the dashed line in Fig. 10 to evidence that the experimental responses were well within the linear region for the operational condition of the element. The response of the first test, marked as Experimental 1, was almost perfectly linear until the brittle failure, while Experimental 2 presented an apparent deviation from linearity at about 5 mm of displacement, followed by a non-linear response until the final failure, which occurred at about 10 mm of displacement.

The failure mode was investigated through an optical microscope analysis on the broken specimens. A curved section is shown in Fig. 8, where the thickening corresponding to the application of the 90° oriented layers is well evidenced in the central zone of the curve. Delaminations were clearly visible starting from the beginning of the thickened zone, at the interface between the 90° oriented layers and the layers of 0° oriented plies. A longitudinal crack was also visible, which passed through the block of 90° oriented layers at the center of the curve and along the internal interface between the 0°- and 90°-oriented plies. According to the visual evidence, failure was likely to be triggered by the development of delamination at the ends of the 90° oriented insert between the internal and external sub-laminates or, alternatively, by the damage onset inside such insert, which then evolved into delaminations.

These tests were also simulated by developing two types of Finite Element models, which are shown in Fig. 9:

- a shell model, which was used to evaluate the reliability of this modeling technique, already adopted for the preliminary design studies presented in the previous sections.
- a ply-wise solid model, which was used as reference solution to validate shell-based modelling technique and for the analysis of the interlaminar state of stress in the curved zones.

The shell model consisted of 2176 bi-linear shells (element S4 [29]) with a typical size of 1.25 mm, while the solid model was developed by using 106,742 quadratic hexahedral element of type *C3D20R* [29] and 6156 quadratic wedge elements of type *C3D15* [29], with a typical size of 0.5 mm.

Considering the comparison between numerical and experimental results, the stiffness of the strip is slightly overestimated by both numerical models. The discrepancies between the numerical and the experimental slopes can be attributed to two fundamental reasons:

i) the numerical models considered only the nominal thickness of the material while in the real component the thickness presents slight variations due to manufacturing imperfection, like resin accumulations in pockets and wrinkles.
ii) the model used the nominal properties of the materials and the nominal orientations, while in the real element the properties were expected to vary depending on the region, since the rectangular plies laminate were stretched to follow the curvatures of the mold changing the density and the orientation of the fibers in the different regions.

Despite the complexity of the real distributions of the reinforcement fibers and of the thickness, the results obtained with nominal parameters were found acceptable for design purposes. Moreover, it can be observed that the shell model obtained very similar results to the solid one, although the latter was more accurate to represent the three-dimensional stress states in the curved parts and in the zones of ply drop off.

The solid model was also be used to investigate the stress state of the element during the test. Fig. 11 shows the contours of σ_{22} stress components and of σ_{33} in correspondence of the experimental load at failure. It can be observed that the σ_{22} stress in 90° oriented inserts at the center of the curved zone do not exceed 30 MPa, while zones of very high interlaminar normal stress concentrations can be seen at the end of the inserts. According to the model, which was developed with the assumption of linear material behavior, both σ_{33} and τ_{13} would have reached non-realistic values, beyond 100 MPa, thus indicating the probable development of interlaminar damage before the ultimate failure. Hence, the numerical results suggest that the delaminations evidenced by the microscope analysis at the end of 90°-oriented insert could have originated the laminate failure. It should also be remarked that the in-plane stress components σ_{11}, σ_{22}, and τ_{12} were lower than the design values defined in Table 5 even at the maximum loads reached in the tests. Moreover, the maximum interlaminar shear stress τ_{13} was found to be about 30 MPa and the maximum normal interlaminar stress σ_{33} was found to be about 20 MPa in limit conditions, without evidencing risk of delamination at limit loads.

Overall, the experiments on the strips confirmed that the quality of the doubly curved corrugate laminate produced was acceptable for the fulfilment of the design requirements, even by adopting the more challenging configuration A, with the lowest period to depth ratio. The numerical analyses indicated that a shell model was adequate for an

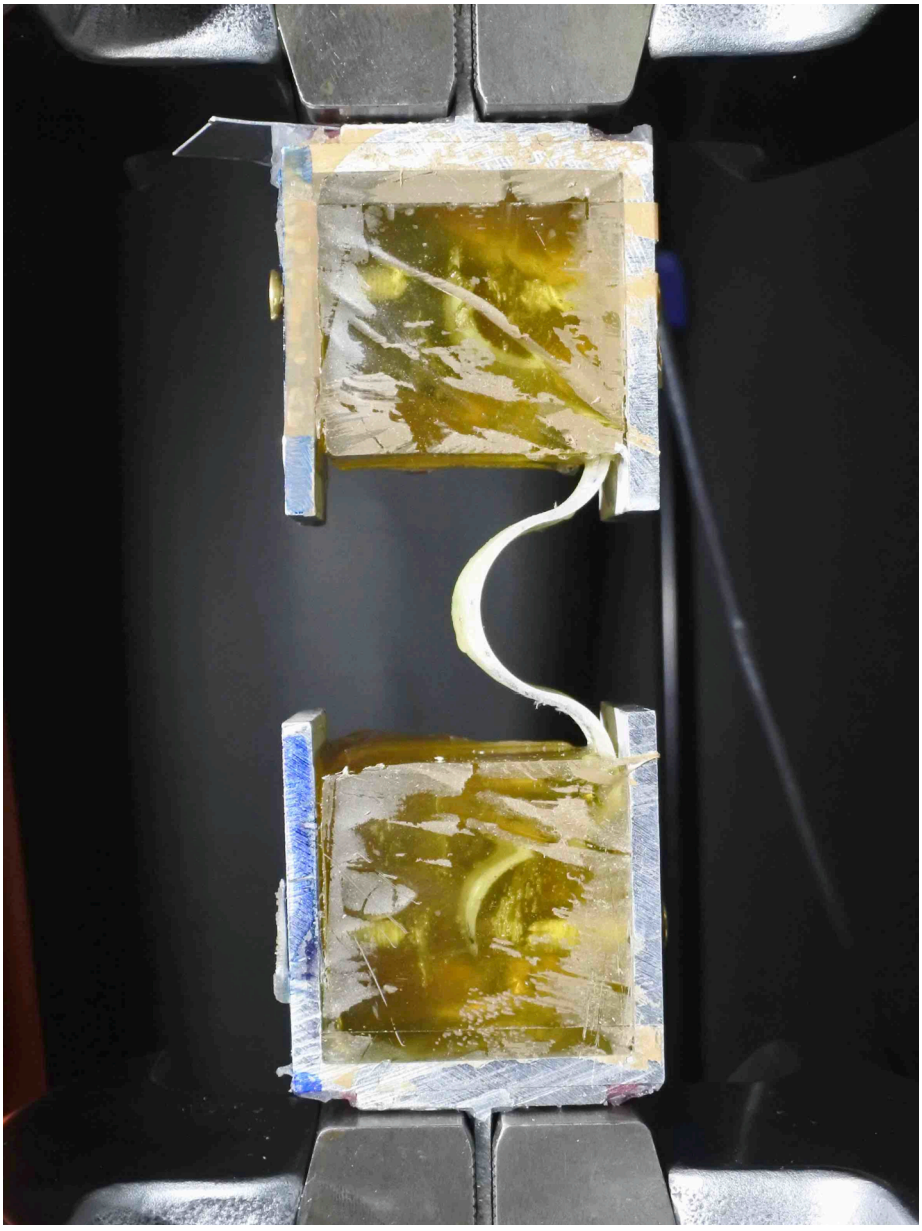

Fig. 7. Specimen during testing.

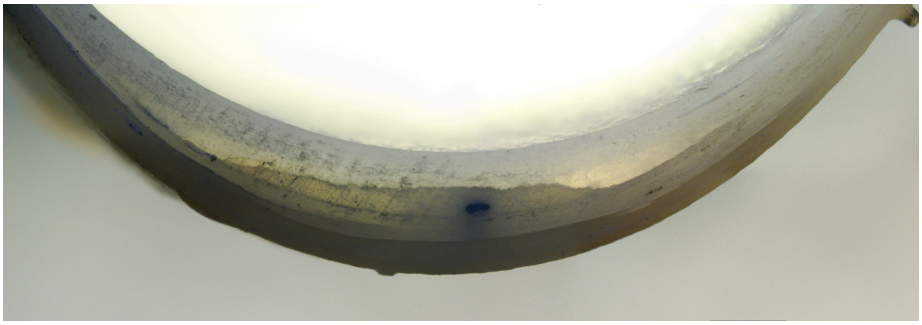

Fig. 8. Interlaminar and intralaminar crack in the broken specimen.

acceptable evaluation of the stiffness of the corrugated modules, despite the uncertainties in fiber distributions and orientations. The final failure was probably determined by interlaminar stress components, which could be captured only by a very detailed solid model, but such phenomenon was predicted for displacements that were significantly higher than those expected in the operational conditions for the joint considered.

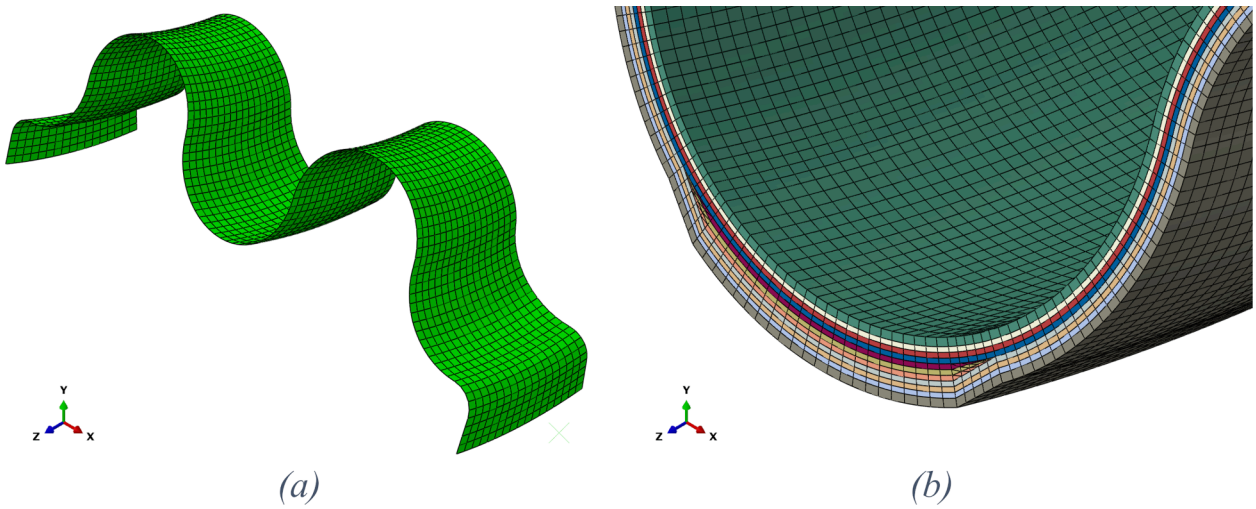

Fig. 9. (a) Shell model; (b) Details of the ply-wise solid model.

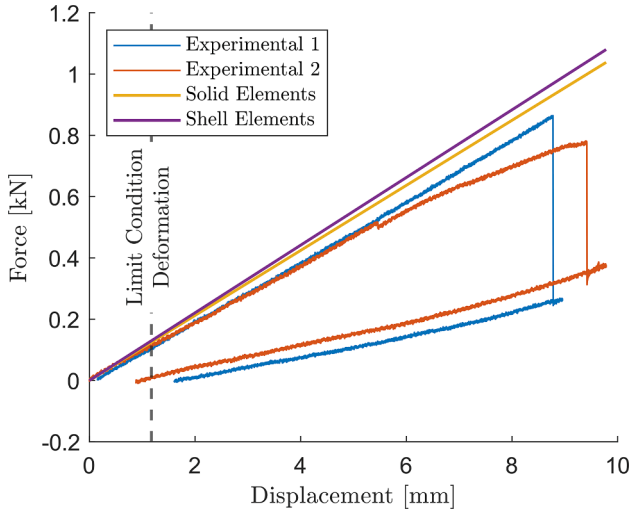

Fig. 10. Testing results with normal operation displacement highlighted.

5. Detailed design, production, and testing of the flexible joint

5.1. Final detailed design of the element

Since the technological trials and the tests provided satisfactory results, the whole joint was designed in detail with the selected geometry and lay-up of the corrugated modules, already assessed in the preliminary module production. In this phase, the details of the metallic frame were defined and the complete configuration was verified numerically.

The stiffeners were designed with flanges and fillets to transmit axial the force between the diaphragms at the end of each module without excessive stress concentrations. The thin webs of the elements were reinforced, in the joint axial direction, using composite strips, to mitigate the risk of local instabilities.

The diaphragms were designed to achieve a desired stiffness in bending and torsion without excessive weight penalties, considering their fundamental role in the transmission of the axial loads between the modules with mutually orthogonal stiffener planes. The cross sections of the annular diaphragms were designed according to a L or T shapes, to provide the surface for the bonding of composite modules.

The sketches of a stiffener for the long central module and of a diaphragm are reported in Fig. 12a and b, respectively.

The stiffeners were provided with flanges with double curvature surface, to match with the surface of the composite corrugated modules. Such flanges were designed to overlap and join, with the use of an adhesive film, the ends of the half-tube. However, the continuity of the load path for torsion and overall strength considerations led to reinforce the longitudinal junctions with the introduction of an internal overlaminate with a [45°] lay-up.

The different parts of the joint were assembled by using aeronautical grade structural adhesive films. The junction line between the diaphragm and the corrugated tubes was found particularly critical in ultimate load conditions, thus suggesting the introduction of external half rings, to be bonded to external surface at the top and the bottom edges of each module, so to completely clamp the border of the composite corrugated laminates. The sketch of the final configuration is presented in Fig. 13.

5.2. Detailed FE of the complete joint

A detailed finite element model was progressively developed during the design phase and guided the identification of the final configuration. The model developed for the Simulia/Abaqus Standard solver is shown in Fig. 14, where the different components are highlighted. It was composed by about 285,000 solid, continuum shell and shell elements, which represented the real geometry for all the parts and also included the modelling of the adhesive layers at the interface between the parts. The corrugated model was created using continuum shell elements *(element SC8R* [29]*)*, while the diaphragm and the constrain rings were modelled by using solid elements *(elements C3D8* [29]*)*. The real geometry was detailly reproduced, including the protruding rings designed to support the borders of the composite corrugated elements. Shell elements were used for the thin internal overlaminates, applied to the internal side of the longitudinal junction between the half-tubes.

The stiffeners were the most complex parts to be modeled due to their geometry characterized by thin and bulk zones. They were modelled through a combination of solid and continuum shell elements (*elements SC8R and C3D8* [29]) to avoid the use of extremely small solid elements for the thin webs, which would have increased the computational cost of the model.

Layers of under integrated solid elements (*elements C3D8R* [29]) were used to represent the adhesive film of about 0.1 mm thickness, to be adopted in physical elements for the final assembly. For each junction line, a layer of solid representing the adhesive was integrated in a conforming mesh of one the parts to be joined. The connection with the other part, with a dissimilar mesh, was obtained by using a TIE connection algorithm available in the solver code.

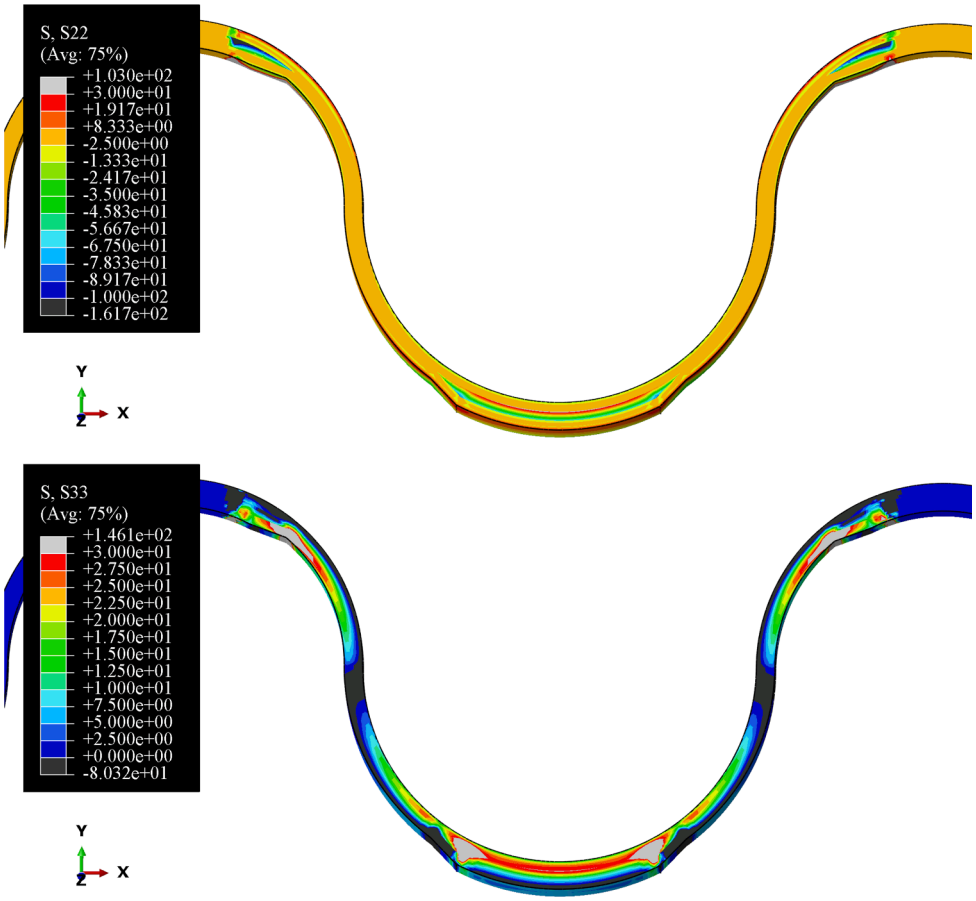

Fig. 11. Stresses at failure.

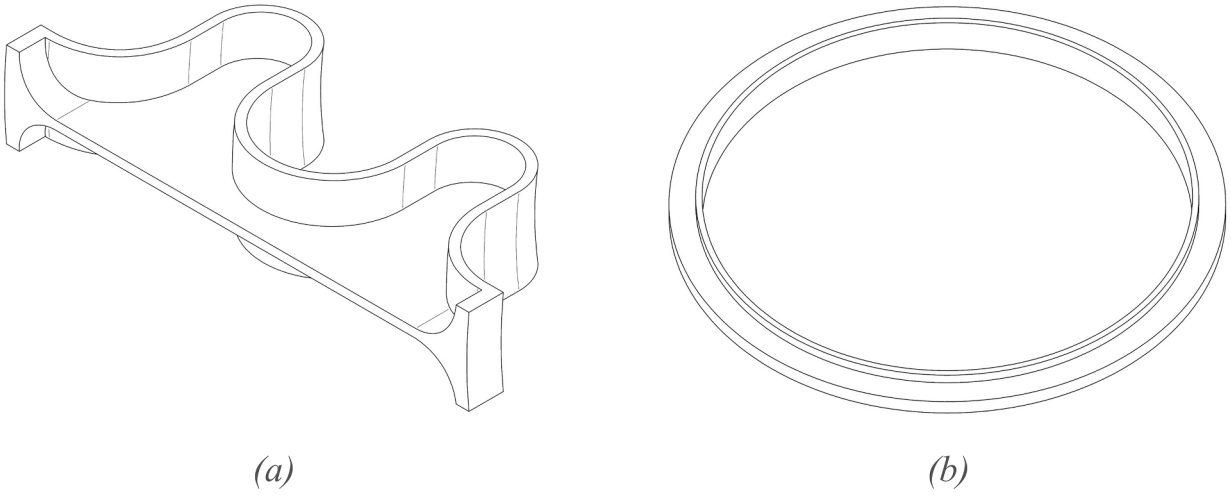

Fig. 12. (a) Stiffeners sketch; (b) Diaphragms sketch.

The layer of solid adhesive representing the adhesive layer was characterized by using an elastic isotropic material model, with E = 3000 MPa and $\nu = 0.3$.

The two diaphragms at the end of the joint were included in two separated rigid bodies and the boundary conditions corresponding to the limit and ultimate load conditions, described in section 3.2, where applied to analyze the state of stress. Moreover, a set of analyses were performed by applying the bending moment along different directions to evaluate the bending stiffness of the joint.

The model was solved by using the limit and ultimate loading conditions. The corrugated element resulted the most critically loaded component. The detailed definition of the metallic frame reduced the severity of the state of stress with respect to the results of the preliminary design reported in section 3. This is confirmed by the results reported in Table 7, which refer to the numerical peak stresses in the corrugated composite parts, normalized with respect to the corresponding design value. It can be observed that design values were not exceeded in limit condition. Regarding the ultimate conditions, the design values were

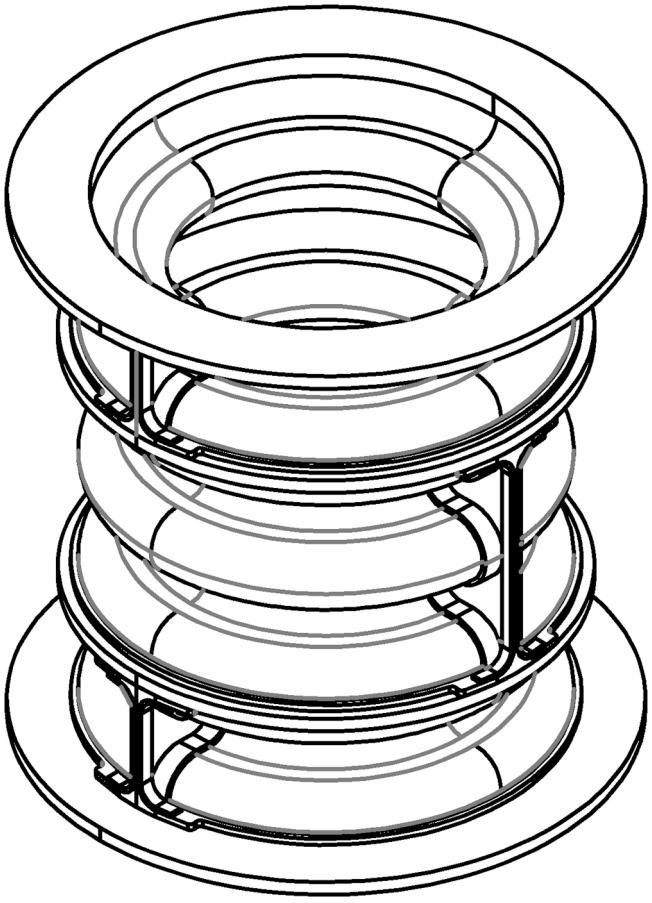

Fig. 13. Sketch of the final configuration.

slightly exceeded, but this was not considered a critical issue, since the region where limits were exceeded was small (see Fig. 15), the design values were conservative with respect to the ultimate strength of the laminates and the ultimate load conditions represent a crash condition that has to be sustained only once in the lifetime of the component. Overall, the analyses showed that the ultimate condition was the most demanding, where both a compressive and torsional load were applied. Although the state of stress was mostly influenced by the compressive component, the analyses indicate that the joint can be subjected to significant compression and torsion, without evidencing risks for the structural integrity, proving that the proposed concept allows the development of a robust design of a flexible joint subjected to a severe load scenario.

5.3. Assembly of a prototype

The production of the six composite half tubes required for the manufacturing of a prototype was carried out by applying the process described in section 4. The metallic parts, namely the stiffeners, the diaphragms, the internal stiffeners, and the half-rings were manufactured in Al 7075 T6 alloy, by machining. The subsequent assembly phase was divided into two parts: the assembly of the main body and the addition of the metallic reinforcement.

The assembly of the main body was carried out in the oven at a temperature of 120 °C with a vacuum bag to apply pressure. To avoid the failure of the composite walls, an internal counter-mold was produced by using silicon rubber. Such central silicon structure was produced by pouring liquid RTV silicone inside a pre-assembly of the joint. Then films of structural adhesive Scotch Weld AFK 163–2 K were applied to the diaphragm surfaces to be bonded to the composite modules, which were assembled. The internal overlaminates were applied along the internal longitudinal junctions, including a final layer of adhesive film to co-bond the overlaminates and the half-tubes.

The stiffeners, the external half-rings to reinforce the junctions between the diaphragms and the composite modules, and the composite reinforcement along the web of the stiffeners were applied with two subsequent curing cycles. Finally, the central silicone was removed, leading to the final joint showed in Fig. 16a.

Overall, the assembly process showed some critical aspects, which led to some imperfections, including wrinkles of overlaminates and gaps between some of the longitudinal junctions. Such defects could have reduced the ultimate strength of the prototype and their presence indicates that improvements are required in the process achieve the ultimate strength levels predicted by the numerical analyses. However, the prototype was considered adequate to test the performances in a pure compressive load condition and to evaluate the stiffness in the different bending directions.

5.4. Bending and compressive tests on the assembled element

Once the assembly procedure was completed, two experimental tests were performed on the complete joint, namely a bending test and an axial compression load. To perform the bending test, eight holes had been previously drilled on the diaphragms at the extremities before the assembly. These holes were placed with a phase of 45° to be able to attach a beam in different directions and place a weight on the beam to apply bending moment, as shown in Fig. 16b. The results of the three bending experiments performed are reported in Fig. 17a. The response of the prototype was linear with small differences between the stiffness in the different bending direction, thus indicating an acceptable quality of the assembly. Actually, the stiffness was not expected to be equal in all the directions, as indicated by the results of the numerical analyses performed on the detailed model of the joint. As expected, the joint respected the requirements imposed on the bending stiffness, with a stiffness well below the maximum acceptable stiffness, which was defined as the stiffness needed to bend the element by 1.4° while applying a moment M_ϑ. The slope corresponding to such limit is indicated by the dash-dot line in Fig. 17a. The comparison between numerical and experimental results indicates that the numerical analyses captured quite well the experimental bending response, especially in the test performed at 0° and 45°. The result is to be considered particularly appreciable, due to the complexity of the design and of the manufacturing process, which introduced significant uncertainties in the geometries.

The structural integrity of the joint under the action of compressive load was evaluated by performing a compressive test, which was carried out by inserting the prototype between two steel flat plates, connected to MTS 858 Mini Bionix II. The test was conducted under displacement control at a speed of 0.25 mm/min.

The force versus displacement obtained in the test is presented in Fig. 17b. An initial non-linearity can be observed at the very beginning of the test, probably originated by an imperfect parallelism between the surfaces of the steel plates and of the external diaphragms. After such initial response, the curve indicates a linear behavior and very limited residual displacement at unloading. The test was continued up to 4 kN, a load that significantly exceeded the compressive load in limit conditions. The picture in Fig. 16c refers to the instant of maximum load. The joint did not present any visible sign of damage both at maximum load and at unloading.

6. Conclusions

The work addressed all the aspects for the development of flexible joints based on axisymmetric composite corrugate laminates with axial and torsional load carrying capabilities. A structural concept was presented, based on the development and the assembly of modules with significant bending compliance along a pre-defined direction and thin-

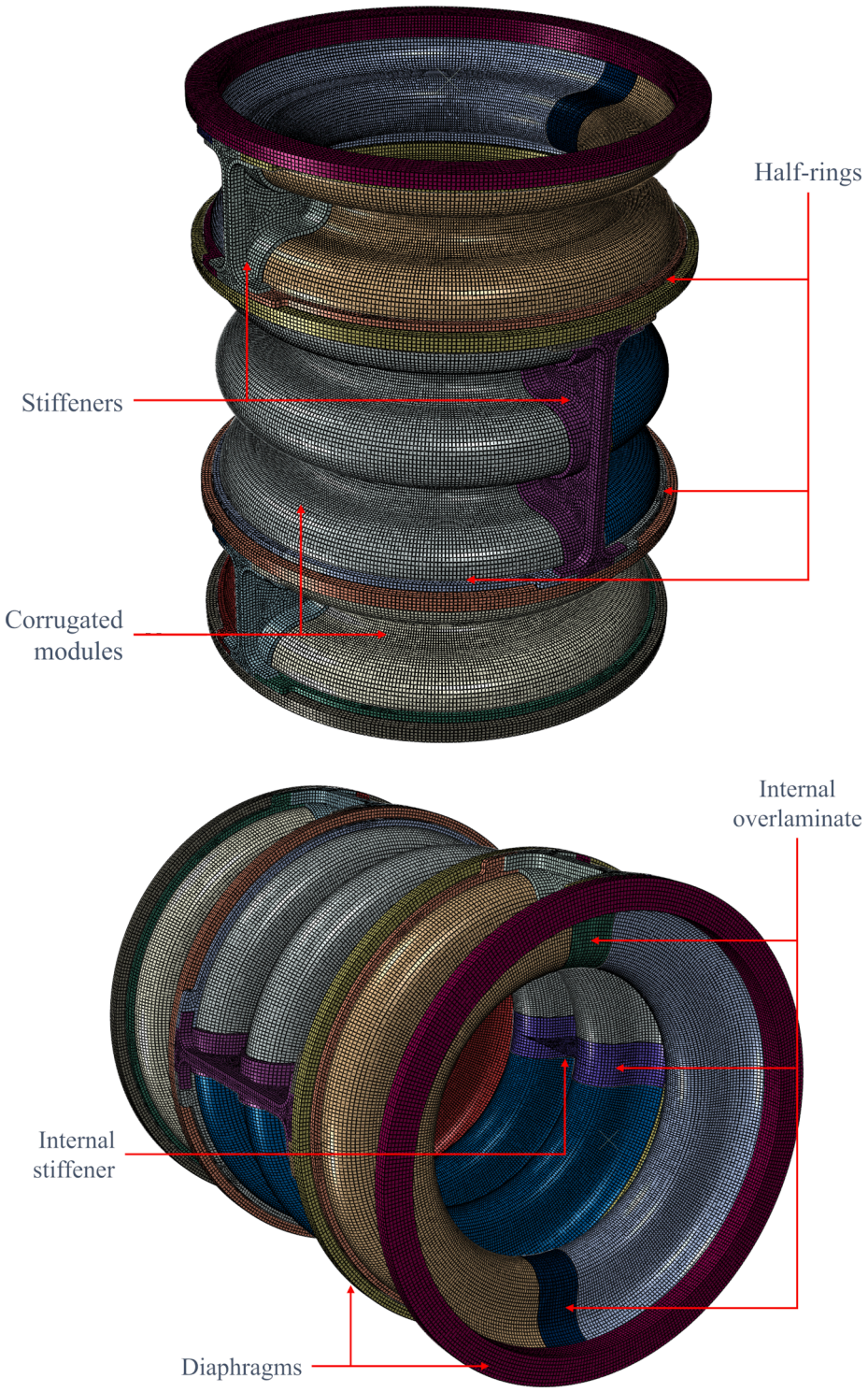

Fig. 14. Detailed model.

Table 7
Peak stresses in the corrugated tube normalized with respect to the corresponding allowable.

	σ_{11}	σ_{22}	σ_{12}	σ_{11}	σ_{22}	σ_{12}
Limit	0.085	0.700	0.424	−0.128	−0.210	−0.424
Ultimate	0.121	1.067	0.818	−0.283	−0.530	−0.939

walled stiffeners working in axial conditions. The preliminary numerical studies confirmed the potential and the design flexibility of the concept, which can be tailored to different requirements. In particular, the key role performed by the corrugated laminate to support the stiffeners, avoiding instability at low critical load was assessed.

An application scenario related to a rotorcraft transmission was considered, which was characterized by complex and severe load conditions and small bending deflections. The design of the joint for the application proposed led to take into consideration the technological challenges related to the production of the joint and to the definition of a

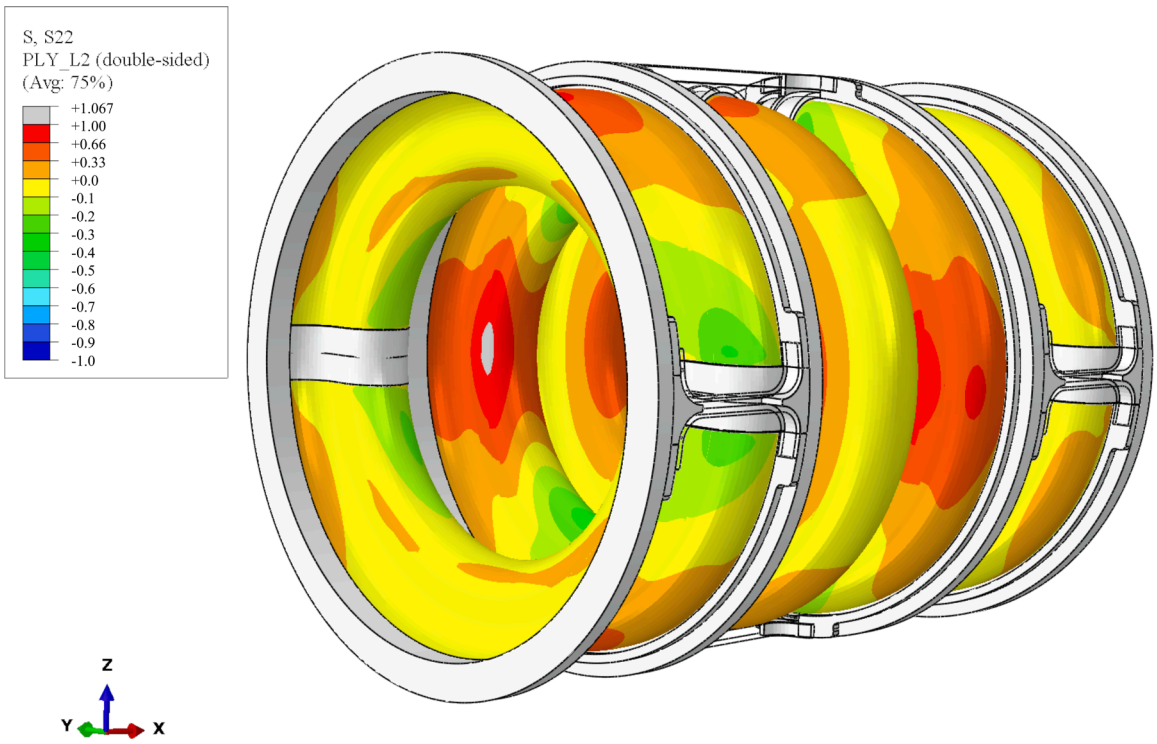

Fig. 15. Stress contour in the tube under ultimate load condition, with a limited region exceeding the allowable value.

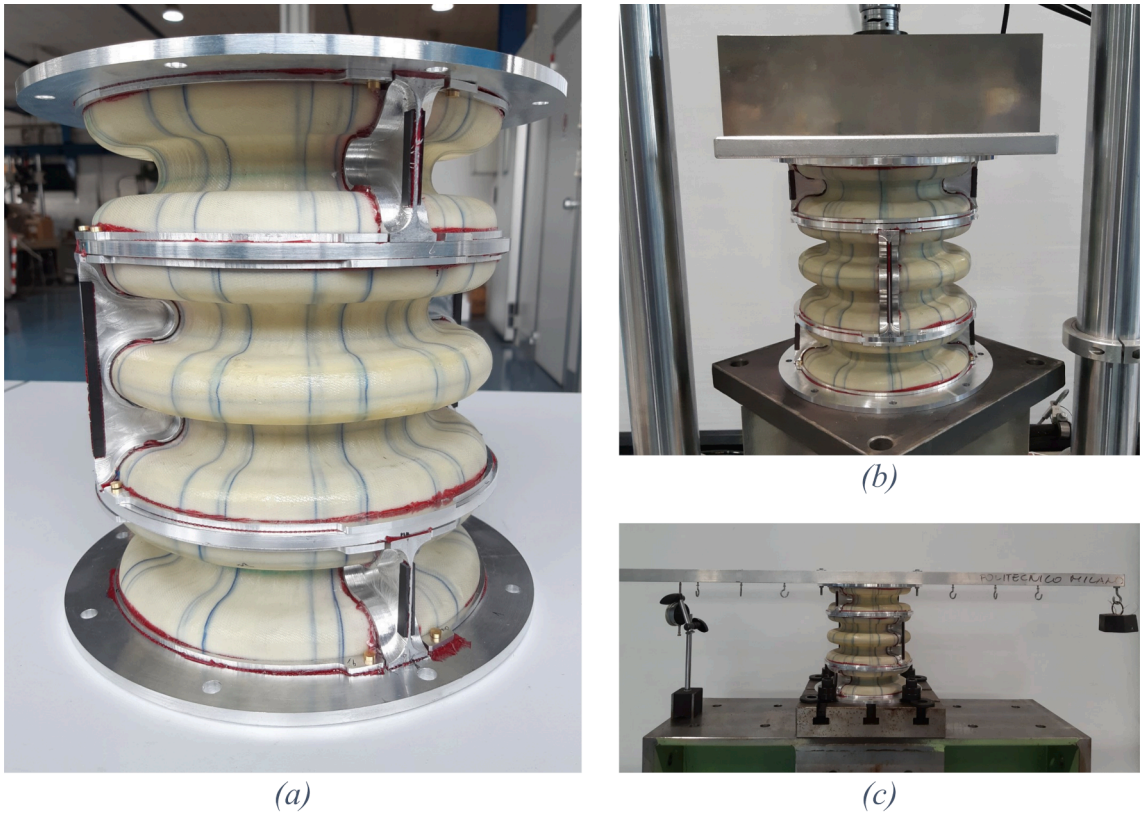

Fig. 16. (a) Complete assembly; (b) Joint in compression test; (c) Joint in bending test.

manufacturing process for axisymmetric composite corrugated laminates, with doubly curved surfaces and multi-directional lay-up. The process, based on the application of elastomeric tooling techniques, led to the production of good quality laminates, as confirmed by the tests performed. Failure was found to be promoted by delamination in the curved zones at significant level of displacements. However, such aspect

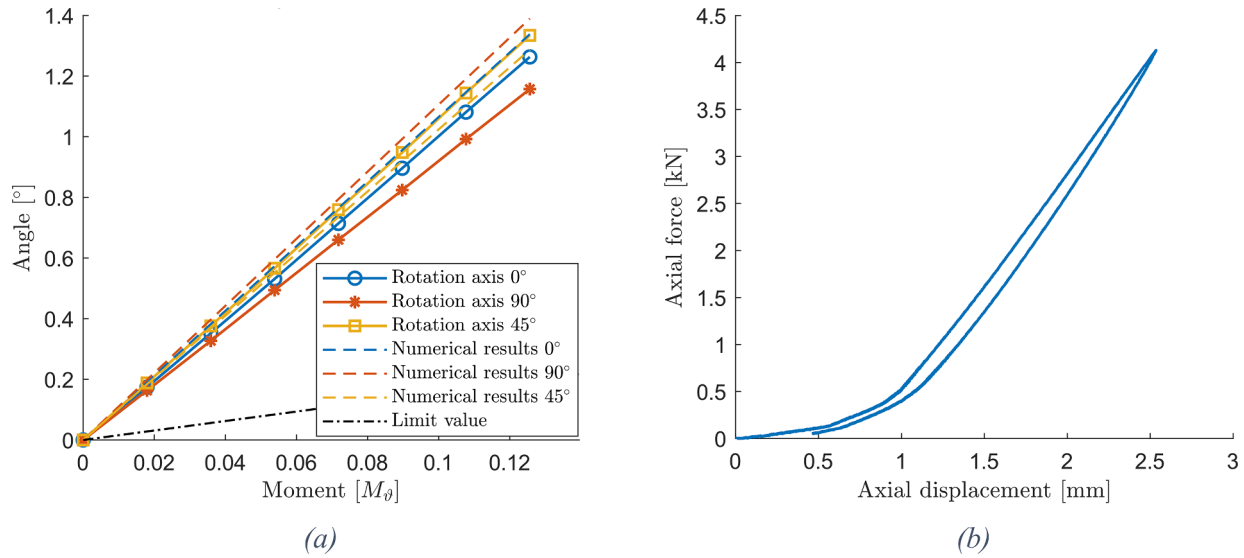

Fig. 17. (a) Experimental results for bending showing the deflection angle over applied moment; (b) Axial tests results reporting the force–displacement curve.

did not represent a critical issue for the application scenario considered, which was characterized by high loads and limited displacement, but it should be taken into account if large bending deflection are required. The comparison with the predictions of numerical models developed at different levels of discretization indicate that the stiffness of the double-curved laminate with variable thickness and lay-up can be approximated at an acceptable level by shell models, although the details of the three-dimensional stress states in the curved zones required the application of solid element within a ply-wise modelling technique.

The final design was supported by the development of a detailed model of the joint, which allowed to define the geometry and the material of the metallic parts that constitute the axial load carrying frame, which was integrated in the composite corrugated tube. The assembly of the whole joint required a quite complex process, which has still to be completely optimized. However, the tests performed on the prototype produced confirmed that the objective of achieving a low bending stiffness in different directions and a considerable load carrying capability was completely achieved, thus pointing out the potential of the structural concept to substitute joints based on heavier and maintenance-demanding mechanisms.

7. Data availability

The raw/processed data required to reproduce these findings cannot be shared due to their confidential nature.

CRediT authorship contribution statement

Marco Riva: Methodology, Formal analysis, Investigation, Writing – original draft. **Alessandro Airoldi:** Conceptualization, Methodology, Writing – review & editing, Supervision, Project administration, Funding acquisition. **Tommaso Turconi:** Methodology, Formal analysis, Investigation. **Pietro Ballarin:** Methodology, Investigation, Writing – original draft. **Matteo Boiocchi:** Conceptualization, Methodology. **Luigi Bottasso:** Conceptualization, Supervision, Project administration, Funding acquisition.

Declaration of Competing Interest

The authors declare the following financial interests/personal relationships which may be considered as potential competing interests: 'Alessandro Airoldi reports financial support and equipment, drugs, or supplies were provided by Leonardo Helicopters Division. Luigi Bottasso has patent #EP3929078A1 HELICOPTER pending to LEONARDO SPA.'

Data availability

The data that has been used is confidential.

Acknowledgements

Funding: This work was funded by Leonardo Helicopters Division.

References

[1] Jensen PDL, Wang F, Dimino I, Sigmund O. Topology optimization of large-scale 3D morphing wing structures. In: Actuators, Vol. 10, No. 9, p. 217. Multidisciplinary Digital Publishing Institute; 2021, September. doi: 10.3390/act10090217.
[2] Lumpe TS, Shea K. Computational design of 3D-printed active lattice structures for reversible shape morphing. J Mater Res 2021;36(18):3642–55. https://doi.org/10.1557/s43578-021-00225-2.
[3] Valasek J. (Ed.). Morphing aerospace vehicles and structures. John Wiley & Sons; 2012.
[4] Concilio A, Lecce L. Historical background and current scenario. In: Concilio A, Dimino I, Lecce L, Pecora R, editors. Morphing wing technologies: Large commercial aircraft and civil helicopters (Chapter 1). Butterworth-Heinemann; 2017. doi: 10.1016/B978-0-08-100964-2.00001-0.
[5] Barbarino S, Bilgen O, Ajaj RM, Friswell MI, Inman DJ. A review of morphing aircraft. J Intell Mater Syst Struct 2011;22(9):823–77. https://doi.org/10.1177/1045389X11414084.
[6] Barbarino S, Flores ES, Ajaj RM, Dayyani I, Friswell MI. A review on shape memory alloys with applications to morphing aircraft. Smart Mater Struct 2014;23(6):063001. https://doi.org/10.1088/0964-1726/23/6/063001.
[7] Sofla AYN, Meguid SA, Tan KT, Yeo WK. Shape morphing of aircraft wing: status and challenges. Mater Des 2010;31(3):1284–92. https://doi.org/10.1016/j.matdes.2009.09.011.
[8] Yokozeki T, Takeda SI, Ogasawara T, Ishikawa T. Mechanical properties of corrugated composites for candidate materials of flexible wing structures. Compos A Appl Sci Manuf 2006;37(10):1578–86. https://doi.org/10.1016/j.compositesa.2005.10.015.
[9] Thill C, Etches JA, Bond IP, Potter KD, Weaver PM. Composite corrugated structures for morphing wing skin applications. Smart Mater Struct 2010;19(12):124009. https://doi.org/10.1088/0964-1726/19/12/124009.
[10] Kress GR, Filipovic DT. Manufacturing and morphing behavior of high-amplitude corrugated laminates. In: Developments and novel approaches in nonlinear solid body mechanics. Cham: Springer; 2020. p. 231–64. https://doi.org/10.1007/978-3-030-50460-1_15.
[11] Kress GR, Filipovic DT. An analytical nonlinear morphing model for corrugated laminates. Curved Layered Struct 2019;6(1):57–67. https://doi.org/10.1515/cls-2019-0005.
[12] Ghabezi P. Rectangular and triangular corrugated composite skins. Fibers Polym 2018;19(2):435–45. https://doi.org/10.1007/s12221-018-7728-8.
[13] Bai JB, Chen D, Xiong JJ, Shenoi RA. A corrugated flexible composite skin for morphing applications. Compos B Eng 2017;131:134–43. https://doi.org/10.1016/j.compositesb.2017.07.056.

[14] Ermakova A, Dayyani I. Shape optimisation of composite corrugated morphing skins. Compos B Eng 2017;115:87–101. https://doi.org/10.1016/j.compositesb.2016.10.029.
[15] Airoldi A, Sala G, Di Landro LA, Bettini P, Gilardelli A. Composite corrugated laminates for morphing applications. In: Concilio A, Dimino I, Lecce L, Pecora R, editors. Morphing wing technologies: Large commercial aircraft and civil helicopters (Chapter 9). Butterworth-Heinemann. doi: 10.1016/B978-0-08-100964-2.00009-5.
[16] Airoldi A, Fournier S, Borlandelli E, Bettini P, Sala G. Design and manufacturing of skins based on composite corrugated laminates for morphing aerodynamic surfaces. Smart Mater Struct 2017;26(4):045024. https://doi.org/10.1088/1361-665X/aa6069.
[17] Airoldi A, Rigamonti D, Sala G, Bettini P, Villa E, Nespoli A. Development of an actuated corrugated laminate for morphing structures. Aeronautical J 2021;125 (1283):180–204. https://doi.org/10.1017/aer.2020.70.
[18] Kang WR, Kim EH, Jeong MS, Lee I, Ahn SM. Morphing wing mechanism using an SMA wire actuator. Int J Aeronaut Space Sci 2012;13(1):58–63. https://doi.org/10.5139/IJASS.2012.13.1.58.
[19] Karagiannis D, Stamatelos D, Spathopoulos T, Solomou A, Machairas T, Chrysohoidis N, et al. Airfoil morphing based on SMA actuation technology. Aircraft Eng Aerospace Technol: Int J 2014. doi: 10.1108/AEAT-10-2012-0194.
[20] Yoshinori T. Rotating shaft (Japanese Patent No. JP2004108441A). Japan Patent Office; 2004.
[21] Koji Y. Steering intermediate shaft for vehicle (Japanese Patent No. JP2004352011A). Japan Patent Office; 2004.
[22] Man L. Flexible transmission shaft (U.S. Patent No. US2006281566A1). United States Patent and Trademark Office; 2006.
[23] Thompson GH. Flexible shafts (UK Patent No. GB1028327A). United Kingdom Intellectual Property Office; 1966.
[24] Takashi M. Flexible transmission shaft (Japanese Patent No. JP2002039149A). Japan Patent Office; 2002.
[25] Ivanovich PG. Flexible shaft (Russian Patent No. RU2106546C1). Russian Federal Service for Intellectual Property; 1998.
[26] Chenzhuo L, Zening G, Zi F, Haoran G, Zhuang F, Zeyu F, et al. Flexible shaft transmission mechanism (Chinese Patent No. CN113062916A). Chinese National Intellectual Property Administration.
[27] Winkler M, Kress G. Deformation limits for corrugated cross-ply laminates. Compos Struct 2010;92(6):1458–68. https://doi.org/10.1016/j.compstruct.2009.11.015.
[28] Schmitz A, Horst P. Bending deformation limits of corrugated unidirectionally reinforced composites. Compos Struct 2014;107:103–11. https://doi.org/10.1016/j.compstruct.2013.07.048.
[29] Dassault Systèmes Simulia. ABAQUS/Standard User's Manual, Version 6.14. Dassault Systèmes Simulia Corp; 2014.
[30] PA 12 - PA2200: Nylon for Industrial 3D Printing | EOS GmbH. Available from: https://www.eos.info/en/additive-manufacturing/3d-printing-plastic/sls-polymer-materials/polyamide-pa-12-alumide (last accessed 10/10/2022).
[31] Department of Defense. MIL-HDBK-17-2F Composite Materials Handbook, Volume 2: Polymer Matrix Composites Materials Properties. Department of Defense. 2002.